arXiv:2009.05295v2 [cond-mat.quant-gas] 20 Jan 2021

Chaos and ergodicity across the energy spectrum of interacting bosons

Lukas Pausch,[1] Edoardo G. Carnio,[1,2] Alberto Rodríguez,[3,*] and Andreas Buchleitner[1,2,†]

[1] *Physikalisches Institut, Albert-Ludwigs-Universität Freiburg, Hermann-Herder-Straße 3, D-79104, Freiburg, Germany*
[2] *EUCOR Centre for Quantum Science and Quantum Computing, Albert-Ludwigs-Universität Freiburg, Hermann-Herder-Straße 3, D-79104, Freiburg, Germany*
[3] *Departamento de Física Fundamental, Universidad de Salamanca, E-37008 Salamanca, Spain*

We identify the chaotic phase of the Bose-Hubbard Hamiltonian by the energy-resolved correlation between spectral features and structural changes of the associated eigenstates as exposed by their generalized fractal dimensions. The eigenvectors are shown to become ergodic in the thermodynamic limit, in the configuration space Fock basis, in which random matrix theory offers a remarkable description of their typical structure. The distributions of the generalized fractal dimensions, however, are ever more distinguishable from random matrix theory as the Hilbert space dimension grows.

Ergodicity, understood as the ability of a system to dynamically explore, irrespective of its initial state, all possible configurations at given energy, is, in general, an exceedingly difficult to prove and rather rare property, at the classical and quantum level [1–3]. On the quantum side, safe ground is established by (intrinsically ergodic [4]) random matrix theory (RMT), which describes systems with classically strictly chaotic ("K-systems" [1–3, 5]) dynamics [6]. RMT predictions for energy spectra and eigenstates [7, 8] define popular benchmarks to certify ergodicity [9, 10].

Ergodicity can, however, emerge on widely variable time scales, hinging on finer structures of phase space, and, at the quantum level, on the effective coarse graining thereof induced by the finite size of $\hbar$ [11]. Since the majority of dynamical systems features mixed rather than strictly chaotic dynamics [12–17], one therefore expects detectable deviations from RMT ergodicity [18, 19], in particular at the level of the eigenvectors' structural properties— which reflect the underlying phase space structure [12–16, 20]. This holds on the level of single as well as of many-body quantum systems, with engineered ensembles of ultracold atoms [21–26] as a modern playground: Notably, interacting bosons on a regular lattice provide a paradigmatic experimental setting to explore the questions above [27–31]; they feature chaos on the level of spectral [32–35] and eigenvector properties [32, 33, 36–39] as well as quench dynamics [40–44].

Here we consider the one-dimensional Bose-Hubbard Hamiltonian (BHH) and combine state-of-the-art numerical simulations with analytical calculations to establish a so far missing integral picture of its chaotic and non-ergodic phases, providing deeper insight into the concept of chaos and ergodicity in the quantum realm. We demonstrate that (i) the energy-resolved chaotic phase is signalled by a clear correlation between spectral features and eigenstate structural changes captured by generalized fractal dimensions (GFD) (cf. Fig. 1), whose fluctuations seem to be qualitatively basis-independent, (ii) a non-ergodic phase persists in the thermodynamic limit, as a function of a scaled tunneling strength, (iii) eigenvectors within the chaotic phase become ergodic in the thermodynamic limit in the configuration space Fock basis, where RMT provides a remarkable description of the eigenstates' typical (i.e., most probable) GFD, (iv) despite such agreement, according to the GFD distributions BHH and RMT depart from each other in an unequivocal statistical sense with increasing size of Hilbert space. This implies that the fluctuations of the eigenstates' structure along the path to ergodicity (even if it be arbitrarily close to RMT at a coarse-grained level) contain statistically robust fingerprints of the specific underlying Hamiltonian.

In terms of standard bosonic operators associated with L Wannier spatial modes, the BHH [45–47] is the sum of a tunneling and a local interaction Hamiltonian with respective strengths J and U,

$$H_{\text{tun}} = -J \sum_k (b_k^\dagger b_{k+1} + b_{k+1}^\dagger b_k), \tag{1}$$

$$H_{\text{int}} = \frac{U}{2} \sum_k n_k \, (n_k - 1) \, . \tag{2}$$

The BHH exhibits a Z_2 symmetry under the reflection operation (Π) about the center of the lattice. In the presence of periodic boundary conditions (PBC), the BHH additionally has translational symmetry, and Hilbert space can be decomposed into L irreducible blocks distinguished by the center-of-mass quasimomentum Q. The $Q = 0$ block further disjoins into symmetric ($\pi = +1$) and antisymmetric ($\pi = -1$) subspaces. For hard-wall boundary conditions (HWBC), the latter π-division applies to the full Hilbert space.

Both H_{tun} and H_{int} are integrable and analytically solvable in appropriate Fock bases. The eigenvectors of the interaction term are the Fock states of the on-site number operators, $|\boldsymbol{n}\rangle \equiv |n_1, \ldots, n_L\rangle$, with $||\boldsymbol{n}||_1 = N$, where N is the number of bosons. The eigenvectors of H_{tun} follow from the Fock states of number operators of spatially delocalized plane-wave or standing-wave modes, for PBC or HWBC, respectively.

The competition between tunneling and interaction makes the BHH non-integrable: For comparable J and U, it exhibits spectral chaos [32–35], identified by short-range spectral measures in accord with the Gaussian orthogonal ensemble (GOE) of RMT. This may be traced back to the underlying classical Hamiltonian [16, 34, 48], whose dynamics are governed by the scaled energy H/UN^2 and the scaled tunneling strength $\eta \equiv J/UN$. In the quantum system, one therefore expects η to control the emergence of chaos in sufficiently dense spectral regions.

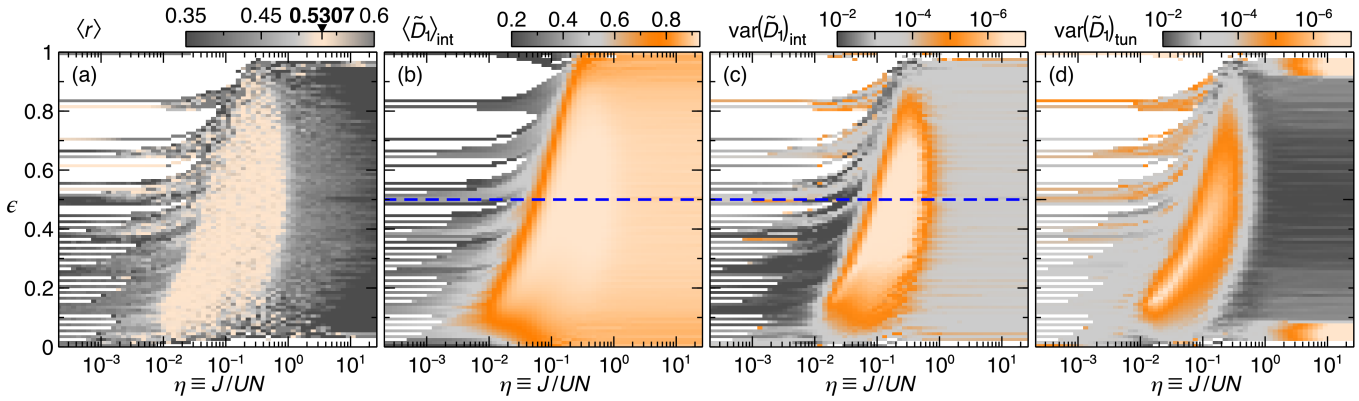


FIG. 1. Evolution of $\langle r\rangle$ (a), $\langle\tilde{D}_1\rangle$ in the eigenbasis of $H_{\rm int}$ (b) and $\mathrm{var}(\tilde{D}_1)$ in the eigenbases of $H_{\rm int}$ (c) and $H_{\rm tun}$ (d), as functions of η and energy $\epsilon = (E - E_{\rm min})/(E_{\rm max} - E_{\rm min})$, for the irreducible Hilbert subspace of size $\mathcal{N} = 55\,898$ with $Q = 0$ and $\pi = -1$, for $N = L = 12$ with PBC. The spectrum was obtained for 75 equally spaced values of $\log_{10}(J/U) \in [-2.92, 3]$, and divided into 100 bins of equal width along the ϵ axis. The value $\langle r\rangle_{\rm GOE}$ is highlighted over the left color bar. Blue dashed lines mark the value $\epsilon = 0.5$ considered in Fig. 2.

We numerically analyze the BHH at unit filling ($N = L$): Eigenstates around chosen energy targets [49–51] as well as full spectra, scaled as $\epsilon \equiv (E - E_{\rm min})/(E_{\rm max} - E_{\rm min}) \in [0, 1]$, enabling the juxtaposition of results for different N and η, are obtained by exact diagonalization. Since the form of $H_{\rm tun}$ and $H_{\rm int}$ reveals that $E_{\rm max} - E_{\rm min} \sim UN^2$ for large N, ϵ effectively provides the classically scaled energy. Short-range statistical features of the spectrum are best captured by the level spacing ratios [52, 53], $r_n = \min(s_{n+1}/s_n, s_n/s_{n+1})$, where $s_n = E_{n+1} - E_n$ is the n-th level spacing. The distributions of r are known approximately analytically for Gaussian random matrix ensembles and accessible numerically without further unfolding procedures, e.g., $\langle r\rangle_{\rm GOE} \approx 0.5307$ [53].

The eigenstate structure of generic many-body Hamiltonians in Hilbert space exhibits multifractal complexity [54–64], and is conveniently described by finite-size generalized fractal dimensions (GFD) [62, 65],

$$\tilde{D}_q \equiv \frac{1}{1-q}\log_{\mathcal{N}} R_q, \quad \text{with} \quad R_q = \sum_\alpha |\psi_\alpha|^{2q}\,, \; q \in \mathbb{R}^+, \tag{3}$$

for eigenvectors with amplitudes ψ_α in a given orthonormal basis of size $\mathcal{N}$. The eigenvector moments are expected to scale asymptotically as $R_q \sim \mathcal{N}^{-(q-1)D_q}$, where the dimensions $D_q \equiv \lim_{\mathcal{N}\to\infty} \tilde{D}_q$ decide whether the state is localized ($D_q = 0$ for $q \geqslant 1$ [66]), multifractal (extended non-ergodic; q-dependent $0 < D_q < 1$), or ergodic ($D_q = 1$ for all q), in the chosen expansion basis. Consequently, the support of ergodic eigenstates—e.g., the eigenvectors of the Wigner-Dyson RMT ensembles [68]—scales asymptotically as the full Hilbert space. Among all GFD, we focus on $\tilde{D}_1$, governing the scaling of the Shannon entropy of $\{|\psi_\alpha|^2\}$, $\tilde{D}_2$, determining the scaling of the eigenstate's inverse participation ratio, and $\tilde{D}_\infty = -\log_{\mathcal{N}} \max_\alpha |\psi_\alpha|^2$, unveiling the extreme statistics of the state's intensities.

We first analyze the connection between spectral chaos and the eigenstates' GFD. In Fig. 1(a)-(c), we show the evolution of $\langle r\rangle$, $\langle\tilde{D}_1\rangle$, and $\mathrm{var}(\tilde{D}_1)$, as functions of scaled energy ϵ and scaled tunneling strength η, for $N = 12$ and PBC (subspace $Q = 0$, $\pi = -1$), evaluated in the eigenbasis of $H_{\rm int}$. The ϵ spectrum is divided into 100 bins of equal width; mean values and variances are computed from eigenvalues and eigenvectors falling into each bin. Energy-resolved density plots expose the coarse-grained level dynamics of the system: Heavily degenerate manifolds of $H_{\rm int}$ fan out as η increases, overlap, and then form a bulk region massively populated by avoided crossings (observable upon finer inspection [69]), which eventually dissolves as the levels reorganize into the bands allowed by $H_{\rm tun}$, for $\eta \gg 1$. We identify a slightly bent oval region of spectral chaos, centered around $\eta \simeq 0.1$ and extending over $0.1 \lesssim \epsilon \lesssim 0.9$, where $\langle r\rangle$ attains the GOE value. This region remains visible after averaging r over a large portion of the bulk spectrum, even without resolving the Π-symmetry [70]. The onset of spectral chaos correlates with a sudden increase in the eigenvectors' GFD, which reach maximum values within the spectral chaos region, as demonstrated for $\langle\tilde{D}_1\rangle$. Strictly simultaneously, the energy-resolved GFD variance undergoes a dramatic reduction by several orders of magnitude. This behavior is also revealed by $\tilde{D}_2$ and $\tilde{D}_\infty$, and qualitatively the same in any irreducible subspace, also for HWBC. The chaotic regime can therefore be identified by the unambiguous correlation between spectral features and structural changes of eigenstates, which, as revealed by the GFD, tend to homogenize their delocalization in Hilbert space, irrespective of their energy.

To elucidate the eigenstates' structural dependence on Hilbert space's size, Fig. 2 shows mean and variance of $\tilde{D}_1$, for fixed $\epsilon = 0.5$ (where the density of states is maximum once spectral chaos kicks in), versus η, for increasing size (up to $\mathcal{N} \approx 2.6 \times 10^6$) of the $\pi = -1$ subspace with HWBC. $\langle\tilde{D}_1\rangle$ registers a surge around $\eta = 0.1$, and reaches a maximum that develops into a distinct plateau, extending towards larger η for increasing L. (Also $\langle r\rangle$ exhibits plateau broadening at $\epsilon = 0.5$ [69].) This behavior is mirrored by the drastic (ever bigger, with increasing L) drop of $\mathrm{var}(\tilde{D}_1)$, with plateaux at its minima. Note that

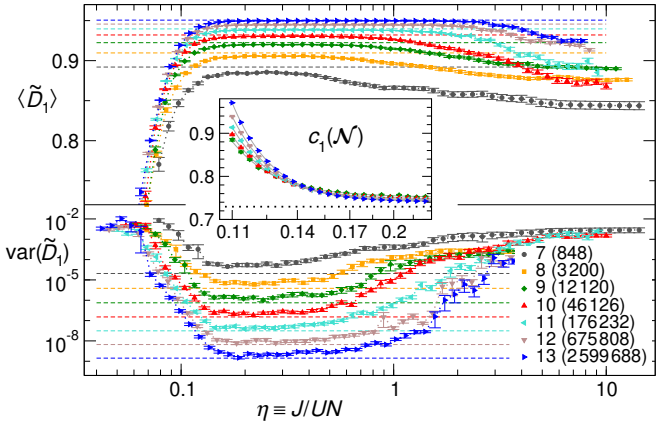


FIG. 2. Evolution of $\langle \tilde{D}_1 \rangle$ (top) and $\mathrm{var}(\tilde{D}_1)$ (bottom) at $\epsilon = 0.5$ versus η, for varying values of L and size ($\mathcal{N}$) (as indicated by the legend) of the subspace spanned by the $\pi = -1$ eigenstates of H_{int} with HWBC. Each data point results from the analysis of the 100 BHH eigenvectors closest to $\epsilon = 0.5$. Corresponding GOE values are indicated by dashed lines. The inset shows the behavior of $c_1(\mathcal{N}) = (1 - \langle \tilde{D}_1 \rangle) \ln \mathcal{N}$ versus η around the crossover region (solid lines are guides to the eye). The horizontal dotted line marks the GOE value of $c_1(\mathcal{N} \to \infty)$.

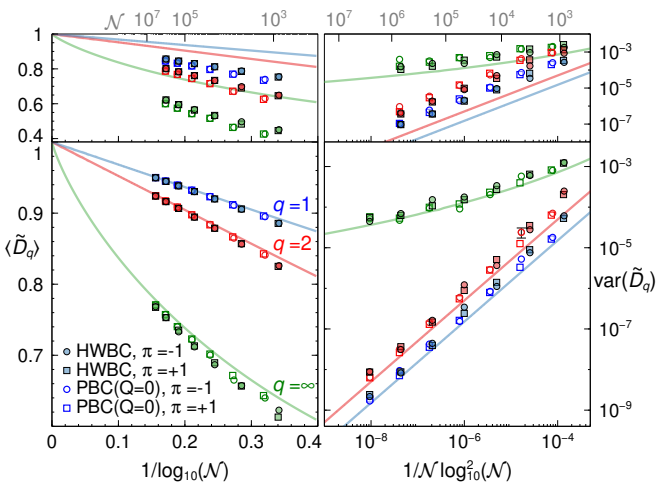


FIG. 3. Average and variance of $\tilde{D}_1$, $\tilde{D}_2$, and $\tilde{D}_\infty$, at $\eta = 0.25$ and $\epsilon = 0.5$, versus size $\mathcal{N}$ of four Hilbert subspaces (distinguished by symbols as indicated; each data point involves 100 eigenstates as in Fig. 2). Lower (upper) panels correspond to the analysis in the eigenbasis of H_{int} (H_{tun}). Solid lines show GOE predictions. Whenever not shown, errors are contained within symbol size.

the plateau values of $\langle \tilde{D}_1 \rangle$ and $\mathrm{var}(\tilde{D}_1)$ agree well with those expected for GOE eigenvectors, indicated by dashed lines in Fig. 2. The same is qualitatively observed for $q = 2, \infty$, other irreducible subspaces, and PBC. The onset of the plateaux appears system size independent in terms of η [70], confirming the relevance of the classically scaled tunneling strength.

To shed further light on the GFD asymptotics within the chaotic region, the lower panels of Fig. 3 show $\langle \tilde{D}_q \rangle$ and $\mathrm{var}(\tilde{D}_q)$ at $\epsilon = 0.5$ and $\eta = 0.25$, for increasing $\mathcal{N}$ of four irreducible subspaces, evaluated in the corresponding eigenbases of H_{int}. The results are compared against the GOE values, which, using known distributions [74] and extreme statistics [75], can be estimated analytically [70]. We find, asymptotically,

$$\langle \tilde{D}_1 \rangle_{\mathrm{GOE}} = 1 - \frac{1}{\ln \mathcal{N}} \left[2 - \gamma - \ln 2 - \frac{1}{\mathcal{N}} + O\left(\mathcal{N}^{-2}\right) \right], \quad (4)$$

$$\langle \tilde{D}_\infty \rangle_{\mathrm{GOE}} = 1 - \frac{\ln(2 \ln \mathcal{N})}{\ln \mathcal{N}} + O\left(\ln \ln \mathcal{N} / \ln^2 \mathcal{N}\right), \quad (5)$$

where γ is Euler's constant, and

$$\mathrm{var}(\tilde{D}_1)_{\mathrm{GOE}} = \frac{1}{\ln^2 \mathcal{N}} \left[\frac{3\pi^2 - 28}{2\mathcal{N}} + O\left(\mathcal{N}^{-2}\right) \right], \quad (6)$$

$$\mathrm{var}(\tilde{D}_\infty)_{\mathrm{GOE}} \sim \ln^{-4} \mathcal{N}. \quad (7)$$

For $q = 2$, we compare the results to the ensemble-averaged GFD, $\langle \tilde{D}_q^{(\mathrm{ens})} \rangle_{\mathrm{GOE}} = \log_{\mathcal{N}} \langle R_q \rangle / (1 - q)$, instead [19][70], with finite-size corrections found identical (up to coefficients) with those for $\tilde{D}_1$. As shown in Fig. 3, the GFD, as well as $\mathrm{var}(\tilde{D}_q)$, in the eigenbasis of H_{int} quickly approach GOE values, independently of subspace or boundary conditions (for the largest $\mathcal{N}$ shown, $\langle \tilde{D}_1 \rangle_{\mathrm{GOE}} - \langle \tilde{D}_1 \rangle = 8 \times 10^{-4}$). The dominant finite-size correction seems to have the same $\mathcal{N}$ dependence for BHH as for GOE eigenvectors, and the GFD show clear evidence of converging to 1 in the thermodynamic limit (as the corresponding variance vanishes). We therefore conclude that the BHH eigenvectors in the chaotic regime become ergodic in the eigenbasis of H_{int} in the thermodynamic limit.

Hence, as $\mathcal{N} \to \infty$, the plateau value of $\langle \tilde{D}_1 \rangle$ in Fig. 2 approaches 1, and, although the crossover into the chaotic region becomes more pronounced with larger L, we cannot definitely determine whether it turns into a sharp transition (i.e., a discontinuity of the derivative with respect to η) or remains smooth and differentiable. The transition features a standard scaling behavior [59, 60, 63, 65] in terms of $c_1(\mathcal{N}) \equiv (1 - \langle \tilde{D}_1 \rangle) \ln \mathcal{N}$: For increasing L, c_1 is unbounded in the non-ergodic phase (where $\langle \tilde{D}_1 \rangle < 1$, i.e., the eigenstates are generically multifractal), and decreases to converge to a constant value in the chaotic phase if the dominant finite-size correction is $\ln^{-1} \mathcal{N}$. That is indeed the behavior observed numerically (inset of Fig. 2), which confirms that the non-ergodic phase for small η persists in the thermodynamic limit. Given the lack of analytical information, we refrain from detailed finite-size scaling analyses on c_1. Nonetheless, close inspection of the tendency of the data locates the transition/crossover, at $\epsilon = 0.5$, in the thermodynamic limit within the region $\eta \in [0.15, 0.2]$ to a reasonable level of confidence. The plateaux's right termination points show no hint of reaching a finite asymptotic value for increasing L, an absence less pronounced for PBC [70]. Although it is appealing to think that an infinitesimal interaction suffices to induce ergodicity in the thermodynamic limit (as discussed for fermions [76]), and hence that the chaotic phase might have no upper η limit (the point $\eta = \infty$ then being a discontinuity), further investigation is necessary to verify such hypothesis.

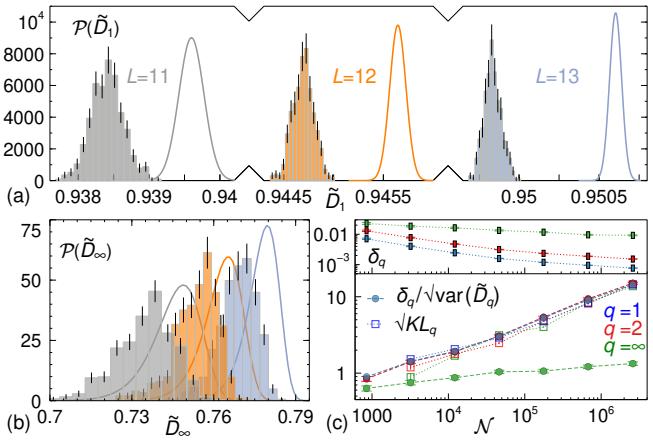


FIG. 4. Evolution of the probability density function of $\tilde{D}_q$ with increasing size $\mathcal{N}$ of the subspace spanned by the $\pi = -1$ eigenstates of $H_{\rm int}$ with HWBC. Panels (a) and (b) display the distributions of $\tilde{D}_1$ and $\tilde{D}_\infty$, respectively, for the indicated L values. Each histogram comprises 500 eigenstates at $\epsilon = 0.5$ in the chaotic domain (100 eigenstates × five values of $\eta \in [0.25, 0.38]$). The $\tilde{D}_1$ distribution for $L = 11$ ($L = 12$) is normalized to 4 (2) for better visualization. Solid lines show GOE distributions [70], the distance to which is evaluated in panels (c), via the difference δ_q of the means (upper plot), the renormalized difference $\delta_q/\sqrt{\mathrm{var}(\tilde{D}_q)}$ and the Kullback-Leibler divergence (lower plot).

Given the demonstrated quality of RMT predictions, one may naively conclude that, at the level of simple eigenvector observables such as Hilbert space (de)localization captured by GFD, as L grows the BHH unequivocally assumes universal RMT behavior within its chaotic phase. But a detailed inspection indicates otherwise: Analysis of the full GFD distributions in Fig. 4 reveals that, although the first and second moments approach the GOE values, the distributions become *more distinguishable* from GOE as L increases. The distance between BHH and GOE distributions is quantified in Fig. 4(c) using the square root of the Kullback-Leibler divergence (relative entropy) [77, 78], $\sqrt{KL_q}$, and $d_q(\mathcal{N}) \equiv \delta_q/\sqrt{\mathrm{var}(\tilde{D}_q)}$, where $\delta_q \equiv \langle \tilde{D}_q \rangle_{\rm GOE} - \langle \tilde{D}_q \rangle$. Both of these measures increase with L for $q = 1, 2, \infty$, demonstrating that, even at the level of the GFD, the two models depart from each other in a statistically unambiguous way: For $\mathcal{N} \gtrsim 10^6$ ($L \geqslant 13, 15$, depending on boundary conditions) the typical $\tilde{D}_{1,2}$ lies more than 10σ away from the most probable GOE value. The distance between the GFD distributions provides valuable information on the finite-size corrections for BHH eigenvectors. Since $\mathrm{var}(\tilde{D}_{1,2}) \sim 1/\mathcal{N}\ln^2\mathcal{N}$, the growth of $d_{1,2}(\mathcal{N})$ with $\mathcal{N}$ entails that $\langle \tilde{D}_{1,2} \rangle$ and $\langle \tilde{D}_{1,2} \rangle_{\rm GOE}$ differ at terms decaying slower than $1/\sqrt{\mathcal{N}}\ln\mathcal{N}$. A data inspection indicates $d_{1,2}(\mathcal{N}) \sim \sqrt{\mathcal{N}}/\ln\mathcal{N}$ as the most likely behavior for large $\mathcal{N}$, implying that $\langle \tilde{D}_{1,2} \rangle$ bear a $1/\ln^2\mathcal{N}$ subleading correction [70]. Note that, for non-overlapping Gaussian distributions of similar width, $\sqrt{KL_q}$ is equivalent to $d_q(\mathcal{N})$. Hence, comparison of these two quantities also provides the distributions' deviation from Gaussianity, as manifestly visible for $q = \infty$.

We finally address the chaotic eigenstates' features' dependence on the expansion basis. Although the GFD are naturally basis dependent, the eigenstates' ergodic character in the thermodynamic limit suggests some degree of invariance under rotations. An analysis performed in the eigenbasis of $H_{\rm tun}$, instead of $H_{\rm int}$, reveals the same qualitative behavior of the energy-resolved $\mathrm{var}(\tilde{D}_q)$ as demonstrated in Fig. 1(d): The GFD fluctuations are strongly suppressed, by several orders of magnitude, and undergo an ever bigger drop for larger system size, within the same parameter region as observed in the $H_{\rm int}$ basis and in the averaged r statistic. Nonetheless, in the eigenbasis of $H_{\rm tun}$, there is no clear identification of a $\langle \tilde{D}_q \rangle$ plateau in the chaotic region [70], and the typical GFD are distant from the GOE values, as shown in the upper panels of Fig. 3. If the GFD in this basis converge to the ergodic limit, too, this is a much slower process governed by stronger finite-size corrections. Such basis dependence reflects the different dynamics that excited eigenstates of $H_{\rm int}$ or of $H_{\rm tun}$ will exhibit under the BHH unitary evolution: While the first display indications of chaos already in relatively small systems [31, 41], the second may be substantially dominated by finite-size/finite-time effects.

We provided an integral view on the chaotic and non-ergodic phases of the Bose-Hubbard Hamiltonian, established by an energy-resolved correlation between spectral features and eigenstate structural changes exposed by the typical values and fluctuations of generalized fractal dimensions. Our results suggest that GFD fluctuations are far more sensitive probes of emergent chaotic behavior than the GFD themselves, and may identify the chaotic phase in any non-trivial basis. In the eigenbasis of the Hamiltonian's interaction part, the chaotic phase eigenvectors become ergodic in the thermodynamic limit, and are remarkably well described by RMT. Yet, in terms of the GFD distributions, their path towards ergodicity turns increasingly more distinguishable from RMT for larger Hilbert spaces, which suggests a statistical handle to discriminate bona fide BHH dynamics in the limit of numerically intractable Hilbert space dimensions. This relates our present results to the field of the certification of distinctive rather than universal features of complex quantum systems [79–82]. Whether this distinct GFD statistics of BHH with respect to RMT can be traced down to unambiguously unique features of the underlying Hamiltonian, or, alternatively, accommodated by more sophisticated random matrix ensembles [83–85], awaits further scrutiny.

We thank J.D. Urbina for helpful discussions, and acknowledge support by the state of Baden-Württemberg through bwHPC and the German Research Foundation (DFG) through Grants No. INST 40/467-1 FUGG (JUSTUS cluster), No. INST 40/575-1 FUGG (JUSTUS 2 cluster), and No. 402552777. E.G.C. acknowledges support from the Georg H. Endress foundation. A.R. acknowledges support by Universidad de Salamanca through a Grant USAL-C1 (No. 18K145).

* argon@usal.es
† a.buchleitner@physik.uni-freiburg.de

[1] A. J. Lichtenberg and M. A. Lieberman, *Regular and Stochastic Motion*, Applied Mathematical Sciences, Vol. 38 (Springer, New York, 1983).
[2] A. M. Ozorio de Almeida, *Hamiltonian Systems: Chaos and Quantization* (Cambridge University Press, Cambridge, 1988).
[3] E. Ott, *Chaos in dynamical systems* (Cambridge University Press, Cambridge, 1993).
[4] A. Pandey, Statistical properties of many-particle spectra: III. Ergodic behaviour in random matrix ensembles, Ann. Phys. (N. Y). **119**, 170 (1979).
[5] O. Bohigas, Random Matrix Theories and Chaotic Dynamics, in *Chaos and Quantum Physics*, École d'été de physique théorique des Houches, Session LII (North Holland, Amsterdam, 1989).
[6] O. Bohigas, M. J. Giannoni, and C. Schmit, Characterization of Chaotic Quantum Spectra and Universality of Level Fluctuation Laws, Phys. Rev. Lett. **52**, 1 (1984).
[7] M. V. Berry, Regular and irregular semiclassical wavefunctions, J. Phys. A Gen. Phys. **10**, 2083 (1977).
[8] D. Delande and J. C. Gay, Quantum Chaos and Statistical Properties of Energy Levels: Numerical Study of the Hydrogen Atom in a Magnetic Field, Phys. Rev. Lett. **57**, 2006 (1986).
[9] I. M. Khaymovich, M. Haque, and P. A. McClarty, Eigenstate Thermalization, Random Matrix Theory, and Behemoths, Phys. Rev. Lett. **122**, 070601 (2019).
[10] G. De Tomasi and I. M. Khaymovich, Multifractality Meets Entanglement: Relation for Nonergodic Extended States, Phys. Rev. Lett. **124**, 200602 (2020).
[11] F. M. Izrailev, Simple models of quantum chaos: Spectrum and eigenfunctions, Phys. Rep. **196**, 299 (1990).
[12] T. Geisel, G. Radons, and J. Rubner, Kolmogorov-Arnol'd-Moser Barriers in the Quantum Dynamics of Chaotic Systems, Phys. Rev. Lett. **57**, 2883 (1986).
[13] O. Bohigas, S. Tomsovic, and D. Ullmo, Manifestations of classical phase space structures in quantum mechanics, Phys. Rep. **223**, 43 (1993).
[14] A. Buchleitner, D. Delande, J. Zakrzewski, R. N. Mantegna, M. Arndt, and H. Walther, Multiple Time Scales in the Microwave Ionization of Rydberg Atoms, Phys. Rev. Lett. **75**, 3818 (1995).
[15] R. Ketzmerick, L. Hufnagel, F. Steinbach, and M. Weiss, New Class of Eigenstates in Generic Hamiltonian Systems, Phys. Rev. Lett. **85**, 1214 (2000).
[16] M. Hiller, T. Kottos, and T. Geisel, Complexity in parametric Bose-Hubbard Hamiltonians and structural analysis of eigenstates, Phys. Rev. A **73**, 061604(R) (2006).
[17] A. A. Michailidis, C. J. Turner, Z. Papić, D. A. Abanin, and M. Serbyn, Slow Quantum Thermalization and Many-Body Revivals from Mixed Phase Space, Phys. Rev. X **10**, 011055 (2020).
[18] H. A. Weidenmüller and G. E. Mitchell, Random matrices and chaos in nuclear physics: Nuclear structure, Rev. Mod. Phys. **81**, 539 (2009).
[19] A. Bäcker, M. Haque, and I. M. Khaymovich, Multifractal dimensions for random matrices, chaotic quantum maps, and many-body systems, Phys. Rev. E **100**, 032117 (2019).
[20] A. R. R. Carvalho and A. Buchleitner, Web-Assisted Tunneling In The Kicked Harmonic Oscillator, Phys. Rev. Lett. **93**, 204101 (2004).
[21] T. Gericke, P. Würtz, D. Reitz, T. Langen, and H. Ott, High-resolution scanning electron microscopy of an ultracold quantum gas, Nat. Phys. **4**, 949 (2008).
[22] M. Karski, L. Förster, J. M. Choi, W. Alt, A. Widera, and D. Meschede, Nearest-Neighbor Detection of Atoms in a 1D Optical Lattice by Fluorescence Imaging, Phys. Rev. Lett. **102**, 053001 (2009).
[23] N. Gemelke, X. Zhang, C. L. Hung, and C. Chin, In situ observation of incompressible Mott-insulating domains in ultracold atomic gases, Nature **460**, 995 (2009).
[24] J. F. Sherson, C. Weitenberg, M. Endres, M. Cheneau, I. Bloch, and S. Kuhr, Single-atom-resolved fluorescence imaging of an atomic Mott insulator, Nature **467**, 68 (2010).
[25] W. S. Bakr, A. Peng, M. E. Tai, R. Ma, J. Simon, J. I. Gillen, S. Fölling, L. Pollet, and M. Greiner, Probing the Superfluid-to-Mott Insulator Transition at the Single-Atom Level, Science **329**, 547 (2010).
[26] F. Meinert, M. J. Mark, K. Lauber, A. J. Daley, and H.-C. Nägerl, Floquet Engineering of Correlated Tunneling in the Bose-Hubbard Model with Ultracold Atoms, Phys. Rev. Lett. **116**, 205301 (2016).
[27] J. P. Ronzheimer, M. Schreiber, S. Braun, S. S. Hodgman, S. Langer, I. P. McCulloch, F. Heidrich-Meisner, I. Bloch, and U. Schneider, Expansion Dynamics of Interacting Bosons in Homogeneous Lattices in One and Two Dimensions, Phys. Rev. Lett. **110**, 205301 (2013).
[28] F. Meinert, M. J. Mark, E. Kirilov, K. Lauber, P. Weinmann, M. Gröbner, and H.-C. Nägerl, Interaction-Induced Quantum Phase Revivals and Evidence for the Transition to the Quantum Chaotic Regime in 1D Atomic Bloch Oscillations, Phys. Rev. Lett. **112**, 193003 (2014).
[29] P. M. Preiss, R. Ma, M. E. Tai, A. Lukin, M. Rispoli, P. Zupancic, Y. Lahini, R. Islam, and M. Greiner, Strongly correlated quantum walks in optical lattices, Science **347**, 1229 (2015).
[30] R. Islam, R. Ma, P. M. Preiss, M. E. Tai, A. Lukin, M. Rispoli, and M. Greiner, Measuring entanglement entropy in a quantum many-body system, Nature **528**, 77 (2015).
[31] A. M. Kaufman, M. E. Tai, A. Lukin, M. Rispoli, R. Schittko, P. M. Preiss, and M. Greiner, Quantum thermalization through entanglement in an isolated many-body system, Science **353**, 794 (2016).
[32] A. R. Kolovsky and A. Buchleitner, Quantum chaos in the Bose-Hubbard model, Europhys. Lett. **68**, 632 (2004).
[33] C. Kollath, G. Roux, G. Biroli, and A. M. Läuchli, Statistical properties of the spectrum of the extended Bose-Hubbard model, J. Stat. Mech. Theory Exp. **2010**, P08011 (2010).
[34] R. Dubertrand and S. Müller, Spectral statistics of chaotic many-body systems, New J. Phys. **18**, 033009 (2016).
[35] D. Fischer, D. Hoffmann, and S. Wimberger, Spectral analysis of two-dimensional Bose-Hubbard models, Phys. Rev. A **93**, 043620 (2016).
[36] W. Beugeling, R. Moessner, and M. Haque, Finite-size scaling of eigenstate thermalization, Phys. Rev. E **89**, 042112 (2014).
[37] W. Beugeling, R. Moessner, and M. Haque, Off-diagonal matrix elements of local operators in many-body quantum systems, Phys. Rev. E **91**, 012144 (2015).
[38] W. Beugeling, A. Andreanov, and M. Haque, Global characteristics of all eigenstates of local many-body Hamiltonians: participation ratio and entanglement entropy, J. Stat. Mech. Theory Exp. **2015**, P02002 (2015).
[39] W. Beugeling, A. Bäcker, R. Moessner, and M. Haque, Statistical properties of eigenstate amplitudes in complex quantum systems, Phys. Rev. E **98**, 022204 (2018).
[40] A. Buchleitner and A. R. Kolovsky, Interaction-Induced Decoherence of Atomic Bloch Oscillations, Phys. Rev. Lett. **91**, 253002 (2003).

[41] S. Sorg, L. Vidmar, L. Pollet, and F. Heidrich-Meisner, Relaxation and thermalization in the one-dimensional Bose-Hubbard model: A case study for the interaction quantum quench from the atomic limit, Phys. Rev. A **90**, 033606 (2014).

[42] C. Kollath, A. M. Läuchli, and E. Altman, Quench Dynamics and Nonequilibrium Phase Diagram of the Bose-Hubbard Model, Phys. Rev. Lett. **98**, 180601 (2007).

[43] G. Roux, Finite-size effects in global quantum quenches: Examples from free bosons in an harmonic trap and the one-dimensional Bose-Hubbard model, Phys. Rev. A **81**, 053604 (2010).

[44] G. Biroli, C. Kollath, and A. M. Läuchli, Effect of Rare Fluctuations on the Thermalization of Isolated Quantum Systems, Phys. Rev. Lett. **105**, 250401 (2010).

[45] M. Lewenstein, A. Sanpera, V. Ahufinger, B. Damski, A. Sen, and U. Sen, Ultracold atomic gases in optical lattices: mimicking condensed matter physics and beyond, Adv. Phys. **56**, 243 (2007).

[46] M. A. Cazalilla, R. Citro, T. Giamarchi, E. Orignac, and M. Rigol, One dimensional bosons: From condensed matter systems to ultracold gases, Rev. Mod. Phys. **83**, 1405 (2011).

[47] K. V. Krutitsky, Ultracold bosons with short-range interaction in regular optical lattices, Phys. Rep. **607**, 1 (2016).

[48] M. Hiller, T. Kottos, and T. Geisel, Wave-packet dynamics in energy space of a chaotic trimeric Bose-Hubbard system, Phys. Rev. A **79**, 023621 (2009).

[49] F. Pietracaprina, N. Macé, D. J. Luitz, and F. Alet, Shift-invert diagonalization of large many-body localizing spin chains, SciPost Phys. **5**, 045 (2018).

[50] S. Balay, S. Abhyankar, M. F. Adams, J. Brown, P. Brune, K. Buschelman, L. Dalcin, A. Dener, V. Eijkhout, W. D. Gropp, D. Karpeyev, D. Kaushik, M. G. Knepley, D. A. May, L. C. McInnes, R. T. Mills, T. Munson, K. Rupp, P. Sanan, B. F. Smith, S. Zampini, H. Zhang, and H. Zhang, *PETSc Users Manual*, Tech. Rep. ANL-95/11 - Revision 3.13 (Argonne National Laboratory, 2020).

[51] V. Hernandez, J. E. Roman, and V. Vidal, SLEPc: A scalable and flexible toolkit for the solution of eigenvalue problems, ACM Trans. Math. Software **31**, 351 (2005).

[52] V. Oganesyan and D. A. Huse, Localization of interacting fermions at high temperature, Phys. Rev. B **75**, 155111 (2007).

[53] Y. Y. Atas, E. Bogomolny, O. Giraud, and G. Roux, Distribution of the Ratio of Consecutive Level Spacings in Random Matrix Ensembles, Phys. Rev. Lett. **110**, 084101 (2013).

[54] J.-M. Stéphan, S. Furukawa, G. Misguich, and V. Pasquier, Shannon and entanglement entropies of one- and two-dimensional critical wave functions, Phys. Rev. B **80**, 184421 (2009).

[55] J.-M. Stéphan, G. Misguich, and V. Pasquier, Rényi entropy of a line in two-dimensional Ising models, Phys. Rev. B **82**, 125455 (2010).

[56] J.-M. Stéphan, G. Misguich, and V. Pasquier, Phase transition in the Rényi-Shannon entropy of Luttinger liquids, Phys. Rev. B **84**, 195128 (2011).

[57] Y. Y. Atas and E. Bogomolny, Multifractality of eigenfunctions in spin chains, Phys. Rev. E **86**, 021104 (2012).

[58] Y. Y. Atas and E. Bogomolny, Calculation of multi-fractal dimensions in spin chains, Phil. Trans. R. Soc. A **372**, 20120520 (2014).

[59] D. J. Luitz, F. Alet, and N. Laflorencie, Universal behavior beyond multifractality in quantum many-body systems., Phys. Rev. Lett. **112**, 057203 (2014).

[60] D. J. Luitz, N. Laflorencie, and F. Alet, Many-body localization edge in the random-field Heisenberg chain, Phys. Rev. B **91**, 081103(R) (2015).

[61] G. Misguich, V. Pasquier, and M. Oshikawa, Finite-size scaling of the Shannon-Rényi entropy in two-dimensional systems with spontaneously broken continuous symmetry, Phys. Rev. B **95**, 195161 (2017).

[62] J. Lindinger, A. Buchleitner, and A. Rodríguez, Many-Body Multifractality throughout Bosonic Superfluid and Mott Insulator Phases, Phys. Rev. Lett. **122**, 106603 (2019).

[63] N. Macé, F. Alet, and N. Laflorencie, Multifractal Scalings Across the Many-Body Localization Transition, Phys. Rev. Lett. **123**, 180601 (2019).

[64] D. J. Luitz, I. Khaymovich, and Y. Bar Lev, Multifractality and its role in anomalous transport in the disordered XXZ spin-chain, SciPost Phys. Core **2**, 006 (2020).

[65] A. Rodriguez, L. J. Vasquez, K. Slevin, and R. A. Römer, Multifractal finite-size scaling and universality at the Anderson transition, Phys. Rev. B **84**, 134209 (2011).

[66] While exponential localization implies vanishing D_q for all $q > 0$, nonexponentially localized states may exhibit $D_q \neq 0$ for some $q < 1$, such as those in a generalized Rosenzweig-Porter model [67].

[67] V. E. Kravtsov, I. M. Khaymovich, E. Cuevas, and M. Amini, A random matrix model with localization and ergodic transitions, New J. Phys. **17**, 122002 (2015).

[68] A. Mirlin, Statistics of energy levels and eigenfunctions in disordered systems, Phys. Rep. **326**, 259 (2000).

[69] L. Pausch, unpublished.

[70] Further information is provided in the Supplemental Material where, additionally, Refs. [71–73] are cited.

[71] Y. V. Fyodorov and O. Giraud, High values of disorder-generated multifractals and logarithmically correlated processes, Chaos, Solitons & Fractals **74**, 15 (2015).

[72] F. W. J. Olver, A. B. Olde Daalhuis, D. W. Lozier, B. I. Schneider, R. F. Boisvert, C. W. Clark, B. R. Miller, B. V. Saunders, H. S. Cohl, and M. A. McClain, NIST Digital Library of Mathematical Functions, http://dlmf.nist.gov/, Release 1.0.27 of 2020-06-15.

[73] O. Giraud, N. Macé, E. Vernier, and F. Alet, Probing symmetries of quantum many-body systems through gap ratio statistics, arXiv:2008.11173 (2020).

[74] F. Haake, S. Gnutzmann, and M. Kuś, *Quantum Signatures of Chaos*, Springer Series in Synergetics (Springer International Publishing, Cham, 2018).

[75] A. Lakshminarayan, S. Tomsovic, O. Bohigas, and S. N. Majumdar, Extreme Statistics of Complex Random and Quantum Chaotic States, Phys. Rev. Lett. **100**, 044103 (2008).

[76] C. Neuenhahn and F. Marquardt, Thermalization of interacting fermions and delocalization in Fock space, Phys. Rev. E **85**, 060101(R) (2012).

[77] S. Kullback and R. A. Leibler, On Information and Sufficiency, Ann. Math. Stat. **22**, 79 (1951).

[78] T. M. Cover and J. A. Thomas, *Elements of Information Theory* (John Wiley & Sons, Hoboken, 2006).

[79] M. C. Tichy, M. Tiersch, F. de Melo, F. Mintert, and A. Buchleitner, Zero-Transmission Law for Multiport Beam Splitters, Phys. Rev. Lett. **104**, 220405 (2010).

[80] L. Aolita, C. Gogolin, M. Kliesch, and J. Eisert, Reliable quantum certification of photonic state preparations, Nat. Commun. **6**, 8498 (2015).

[81] T. Giordani, F. Flamini, M. Pompili, N. Viggianiello, N. Spagnolo, A. Crespi, R. Osellame, N. Wiebe, M. Walschaers, A. Buchleitner, and F. Sciarrino, Experimental statistical signature of many-body quantum interference, Nat. Photonics **12**, 173 (2018).

[82] T. V. Zache, T. Schweigler, S. Erne, J. Schmiedmayer, and J. Berges, Extracting the Field Theory Description of a Quantum Many-Body System from Experimental Data, Phys. Rev. X **10**, 011020 (2020).

[83] K. Mon and J. French, Statistical properties of many-particle spectra, Ann. Phys. (N. Y.). **95**, 90 (1975).
[84] L. Benet and H. A. Weidenmüller, Review of the k -body embedded ensembles of Gaussian random matrices, J. Phys. A. Math. Gen. **36**, 3569 (2003).
[85] N. D. Chavda and V. K. B. Kota, Localization-delocalization transitions in bosonic random matrix ensembles, Ann. Phys. **529**, 1600287 (2017).

Supplemental Material

Chaos and ergodicity across the energy spectrum of interacting bosons

FURTHER RESULTS ON SPECTRAL FEATURES AND EIGENSTATE STRUCTURE OF THE BHH

Table I lists the sizes of the different irreducible Hilbert spaces considered in our numerical analysis. It is worth noting that while in the basis of $H_{\rm int}$ the number of non-zero elements per row in the Hamiltonian matrix grows linearly with L, the sparsity is severely reduced in the basis of $H_{\rm tun}$, where the number of non-zeros scales as L^3, which makes the numerical treatment far more demanding. The analysis in the tunneling eigenbasis is restricted to $L \leqslant 12$ ($L \leqslant 14$) for hard-wall (periodic) boundary conditions.

The average over the energy axis of the level statistics, as usually considered in the literature [32–35], also reveals the existence of spectral chaos. Figure S1 shows the level spacing ratio averaged over the inner 70% of the eigenenergies as a function of $\eta \equiv J/UN$ for varying system sizes with hard-wall boundary conditions. Agreement with the results expected for GOE eigenvalues is clearly observed within a range of the interaction strength which correlates with the behavior shown in Fig. 1. The region of spectral chaos is also visible even upon consideration of the full Hilbert space, i.e., without resolving the symmetric and antisymmetric subspaces induced by the reflection symmetry about the center of the chain.

As can be seen in Fig. 2 of the manuscript, the upper limit of the $\langle \tilde{D}_1 \rangle$ plateau seems to keep increasing for larger L. To quantify that behavior, we estimate the lower and upper limits of the plateaux as the positions where the difference between the typical GFD value and the corresponding GOE value is twice the minimum difference between these two, and show their evolution as functions of Hilbert space size for different boundary conditions in Fig. S2. While the lower limit, η_L, converges to a value in the region $[0.15, 0.2]$ for all the cases considered, the upper limit, η_U, does not exhibit an asymptotic saturation (especially for HWBC) in the accessible range of $\mathcal{N}$.

The energy-resolved correlation between the spectral statistics and the eigenvector structure in the eigenbasis of $H_{\rm tun}$, as function of rescaled energy ϵ and hopping strength η, is presented for $\langle \tilde{D}_1 \rangle$ in Fig. S3, and should be compared against Fig. 1 in the manuscript. To illustrate similarities and differences between the two bases, the color scales were chosen exactly identical in both figures. Note that the overall evolution of the values of the GFD is inverted as compared to the analysis in the $H_{\rm int}$ basis, since the eigenvectors must be highly localized in the limit $\eta \to \infty$. The evolution of var$(\tilde{D}_q)$ in the $H_{\rm tun}$ eigenbasis shows a region of drastically suppressed GFD fluctuations that agrees with the corresponding area observed in Fig. 1. The inspection of $\langle \tilde{D}_1 \rangle$ at $\epsilon = 0.5$, shown in Fig. S4, does not reveal the clear formation of a plateau, and the typical GFD values are rather far from the RMT prediction, as also illustrated in Fig. 3 of the manuscript. Despite the basis dependence of the typical GFD, their fluctuations might be a basis-independent figure of merit to identify the emergence of a chaotic regime.

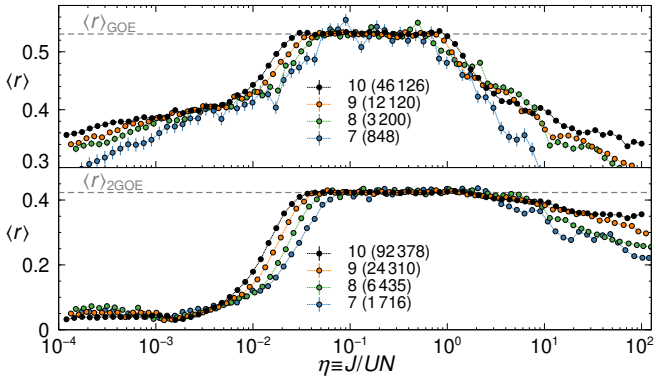


FIG. S1. Average of r over the inner 70% of the eigenenergies as a function of η for varying values of L and size ($\mathcal{N}$) (as indicated by the legend) of the reflection-antisymmetric subspace (top) as well as of the full Hilbert space with hard-wall boundary conditions. Expected results for GOE eigenvalues (top) and two superimposed GOE spectra (bottom) are indicated by dashed lines. $\langle r \rangle_{\rm 2GOE} = 0.4232 \pm 0.0002$ was obtained numerically by simulating 1000 realizations of the superimposed spectra of two 1000×1000 GOE random matrices and agrees well with recent analytical predictions [73].

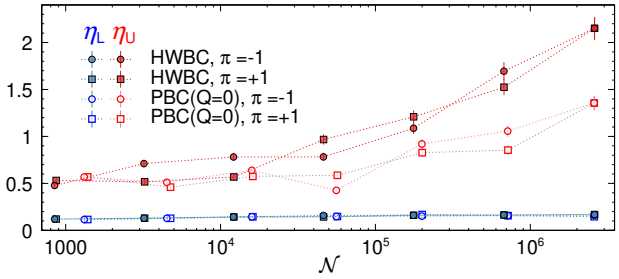


FIG. S2. Estimation of the lower (η_L) and upper (η_U) limits of the $\langle \tilde{D}_1 \rangle$ plateau at $\epsilon = 0.5$ versus Hilbert space size, for four irreducible spaces resulting from the combination of translation and reflection symmetries, distinguished by different symbols as indicated in the plot.

L	7	8	9	10	11	12	13	14	15
HWBC, $\pi=-1$	848	3200	12 120	46 126	176 232	675 808	2 599 688		
HWBC, $\pi=+1$	868	3235	12 190	46 252	176 484	676 270	2 600 612		
PBC ($Q=0$), $\pi=-1$			1317	4500	15 907	55 898	199 550	714 714	2 583 586
PBC ($Q=0$), $\pi=+1$			1387	4752	16 159	56 822	200 474	718 146	2 587 018

TABLE I. Size of the analyzed irreducible Hilbert spaces as function of L.

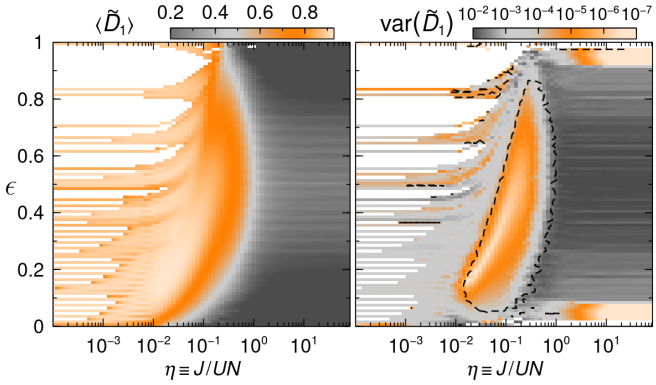


FIG. S3. Evolution of $\langle\tilde{D}_1\rangle$ (left) and var($\tilde{D}_1$) (right) as functions of η and rescaled energy $\epsilon = (E - E_{\rm min})/(E_{\rm max} - E_{\rm min})$, for the irreducible subspace of size $\mathcal{N} = 55\,898$ spanned by the $Q = 0$ and $\pi = -1$ eigenbasis of $H_{\rm tun}$ for $N = L = 12$ with PBC (cf. Fig. 1 in manuscript). The black dashed line in the right panel indicates the contour var($\tilde{D}_1$) $= 5 \times 10^{-5}$ for the analysis in the eigenbasis of $H_{\rm int}$, shown in Fig. 1 of the manuscript. The color scales for $\langle\tilde{D}_1\rangle$ and var($\tilde{D}_1$) are exactly the same as those used in Fig. 1 of the manuscript.

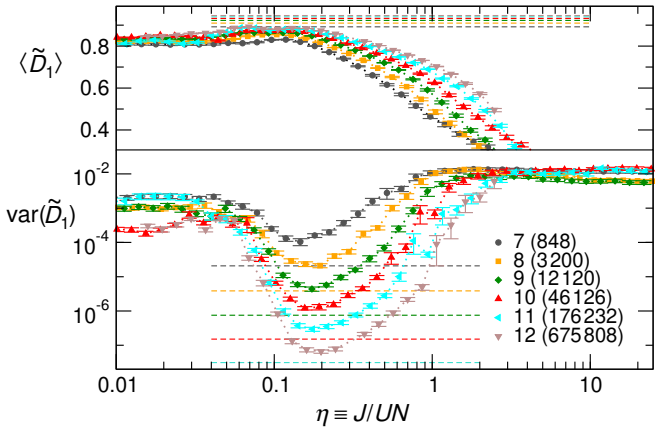


FIG. S4. Evolution of $\langle\tilde{D}_1\rangle$ (top) and var($\tilde{D}_1$) (bottom) at $\epsilon = 0.5$ versus η, for varying values of L and size ($\mathcal{N}$) (as indicated by the legend) of the subspace spanned by the $\pi = -1$ eigenstates of $H_{\rm tun}$ with HWBC. Each data point results from the analysis of the 100 BHH eigenvectors closest to $\epsilon = 0.5$. Corresponding GOE values are indicated by dashed lines.

GENERALIZED FRACTAL DIMENSIONS FOR GOE EIGENVECTORS

Since $\tilde{D}_1 = -(\ln \mathcal{N})^{-1} \sum_\alpha |\psi_\alpha|^2 \log_{\mathcal{N}} |\psi_\alpha|^2$, the calculation of its mean and variance can be carried out exactly from the known one- and two-intensity distributions of GOE eigenvectors [74]. For $q = 2$, the analytical calculations for the typical GFD are rather challenging, but the results for the ensemble-averaged GFD (obtained from the arithmetic average of the R_q moments, i.e., $\langle\tilde{D}_2^{(\rm ens)}\rangle = -\log_{\mathcal{N}}\langle R_2\rangle$) provide excellent approximations [19],

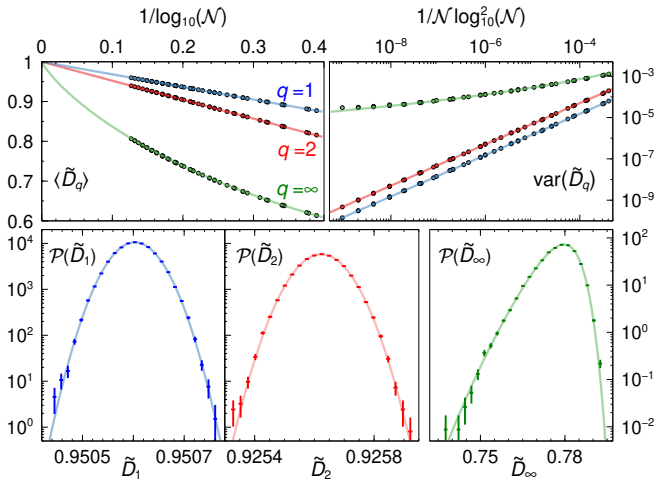


FIG. S5. Comparison between analytical and numerical results for the GFD of GOE eigenvectors. Average and variance of $\tilde{D}_q$ as a function of the vector length $\mathcal{N}$ are shown in the upper panels, while the lower plots display probability density functions of $\tilde{D}_q$ for $\mathcal{N} = 2\,599\,688$. Solid lines follow from the evaluation of Eqs. (S1)-(S8); symbols and error crosses (indicating $\pm 1\sigma$) are obtained from the numerical sampling of GOE eigenvectors [10^4 for $\langle\tilde{D}_q\rangle$, var($\tilde{D}_q$), and 5×10^4 for the distributions].

$$\langle\tilde{D}_1\rangle_{\rm GOE} = \frac{H_{\mathcal{N}/2} - 2 + \ln 4}{\ln \mathcal{N}}, \tag{S1}$$

$$\langle\tilde{D}_2^{(\rm ens)}\rangle_{\rm GOE} = \frac{\ln(\mathcal{N}+2) - \ln 3}{\ln \mathcal{N}}, \tag{S2}$$

where $H_n = \sum_{k=1}^{n} \frac{1}{k}$ is the harmonic number, and

$$\mathrm{var}(\tilde{D}_1) = \frac{(3\pi^2 - 24)(\mathcal{N}+2) - 8}{2(\mathcal{N}+2)^2 \ln^2 \mathcal{N}} - \frac{\psi^{(1)}(2 + \mathcal{N}/2)}{\ln^2 \mathcal{N}}, \tag{S3}$$

$$\mathrm{var}(\tilde{D}_2^{(\rm ens)}) = \frac{8(\mathcal{N}-1)}{3(\mathcal{N}+4)(\mathcal{N}+6)\ln^2(\mathcal{N})}, \tag{S4}$$

where $\psi^{(1)}$ denotes the first derivative of the digamma function (see Eq. 5.2.2 in Ref. [72]). We emphasize the importance of using the two-intensity distribution to calculate the variance

of $\tilde{D}_1$. The correlation among the intensities induced by normalization plays a crucial role in obtaining the correct result. The validity of Eqs. (S1)-(S4) is borne out by the numerical data (cf. Fig. S5).

We found that the probability density functions of $\tilde{D}_1$ and $\tilde{D}_2$ are very well described by Gaussians with the corresponding mean and variance given above, as demonstrated in Fig. S5.

For $q = \infty$, we deal with the extreme statistics of the eigenvector intensities. In this case, one can proceed in the way suggested in Ref. [75]. In order to find the distribution for the variable $t \equiv \max_\alpha |\psi_\alpha|^2$, we neglect the correlation among the intensities induced by the eigenstate normalization (such correlation does not seem to be crucial in this case). From the Porter-Thomas distribution $P(|\psi_\alpha|^2)$ for the wavefunction intensities for large $\mathcal{N}$ [74] the cumulative distribution function of t thus reads $F(t,\mathcal{N}) = \prod_{\alpha=1}^{\mathcal{N}} \int_0^t \mathrm{d}\,|\psi_\alpha|^2 \;\; P(|\psi_\alpha|^2) = \left[\mathrm{Erf}(\sqrt{t\mathcal{N}/2})\right]^{\mathcal{N}}$, and consequently its PDF can be written as

$$\rho(t,\mathcal{N}) = \frac{\mathcal{N}^{3/2}}{\sqrt{2\pi t}} e^{-t\mathcal{N}/2} \left[\mathrm{Erf}(\sqrt{t\mathcal{N}/2})\right]^{\mathcal{N}-1}. \qquad \text{(S5)}$$

The PDF for $\tilde{D}_\infty = -\log_{\mathcal{N}} t$ is thus given by

$$\mathcal{P}(\tilde{D}_\infty) = \rho(\mathcal{N}^{-\tilde{D}_\infty}, \mathcal{N})\, \mathcal{N}^{-\tilde{D}_\infty} \ln \mathcal{N}, \qquad \text{(S6)}$$

which is in excellent agreement with the numerics, as we demonstrate in Fig. S5. After doing an appropriate change of variable and integrating by parts (neglecting one term that decreases exponentially with $\mathcal{N}$), one can estimate the moments of $\tilde{D}_\infty$ from

$$\langle \tilde{D}_\infty^k \rangle = \frac{(-1)^{k-1} 2k}{\ln^k \mathcal{N}} \int_{1/\sqrt{2}}^{\sqrt{\mathcal{N}/2}} dx \frac{[\mathrm{Erf}(x)]^{\mathcal{N}}}{x} \ln^{k-1}(2x^2/\mathcal{N}). \qquad \text{(S7)}$$

After an adequate treatment of $[\mathrm{Erf}(x)]^{\mathcal{N}}$ for large $\mathcal{N}$, we find for $k = 1$

$$\langle \tilde{D}_\infty \rangle_{\mathrm{GOE}} = 1 - \frac{\ln(2\ln\mathcal{N})}{\ln\mathcal{N}} + \frac{\ln(\ln^2(2)\pi\ln\mathcal{N})}{2\ln^2\mathcal{N}} + O\left(\ln^2\ln\mathcal{N}/\ln^3\mathcal{N}\right), \qquad \text{(S8)}$$

which provides a remarkable description of the numerical data, as shown in Fig. S5. It is worth noting that the leading correction for $\tilde{D}_\infty$ exhibits the generic dependence expected for the extreme statistics of multifractal eigenvectors [71]. The calculation of the leading terms of the second moment, and thus of the variance, proves to be more involved, although analytical inspection suggests that $\mathrm{var}(\tilde{D}_\infty)_{\mathrm{GOE}} \sim \ln^{-4}\mathcal{N}$ as $\mathcal{N} \to \infty$. In any case, $\langle \tilde{D}_\infty^2 \rangle$ can be estimated by evaluating numerically Eq. (S7).

DEPARTURE OF $\mathcal{P}(\tilde{D}_q)$ FROM GOE AND FINITE-SIZE CORRECTIONS TO $\langle \tilde{D}_q \rangle$

The behavior of the distance between the GFD distributions for BHH and GOE eigenvectors, evaluated via

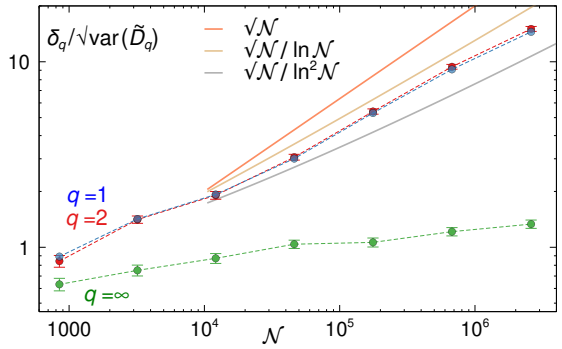


FIG. S6. Distance $\delta_q/\sqrt{\mathrm{var}(\tilde{D}_q)}$ between the distributions of $\tilde{D}_q$ for the BHH and GOE eigenvectors as a function of $\mathcal{N}$, as shown in panel (c) of Fig. fig:PDFs in the manuscript. Solid lines indicate different functional dependencies of the form $\sqrt{\mathcal{N}}/\ln^{n-1}\mathcal{N}$, for $n = 1, 2, 3$.

$d_q(\mathcal{N}) \equiv \delta_q/\sqrt{\mathrm{var}(\tilde{D}_q)}$, reveals how the finite-$\mathcal{N}$ corrections in $\langle \tilde{D}_q \rangle$ and $\langle \tilde{D}_q \rangle_{\mathrm{GOE}}$ differ from each other. For $q = 1, 2$, the numerical data shows that the leading correction to both $\langle \tilde{D}_q \rangle$ and $\langle \tilde{D}_q \rangle_{\mathrm{GOE}}$ is $\sim 1/\ln\mathcal{N}$. If the coefficient of this term differs slightly between BHH and GOE, it ensues that $\delta_q \equiv \langle \tilde{D}_q \rangle_{\mathrm{GOE}} - \langle \tilde{D}_q \rangle \sim 1/\ln\mathcal{N}$. Since $\sqrt{\mathrm{var}(\tilde{D}_q)} \sim 1/\sqrt{\mathcal{N}}\ln\mathcal{N}$, this would lead to

$$d_q(\mathcal{N}) \sim \sqrt{\mathcal{N}}. \qquad \text{(S9)}$$

On the other hand, if the leading term coincides for both models, then δ_q will scale as the dominant subleading term in either $\langle \tilde{D}_q \rangle$ or $\langle \tilde{D}_q \rangle_{\mathrm{GOE}}$. Assuming subleading corrections in the BHH of the form $\ln^{-n}\mathcal{N}$, $n \geq 2$, one obtains

$$d_q(\mathcal{N}) \sim \frac{\sqrt{\mathcal{N}}}{\ln^{n-1}\mathcal{N}}. \qquad \text{(S10)}$$

Alternatively, if the first subleading term to $\langle \tilde{D}_q \rangle$ had the same functional dependence on $\mathcal{N}$ as for GOE, one would find $\delta_q \sim 1/\mathcal{N}\ln\mathcal{N}$ and hence

$$d_q(\mathcal{N}) \sim \frac{1}{\sqrt{\mathcal{N}}}, \qquad \text{(S11)}$$

which would decrease with $\mathcal{N}$, in contrast to the numerically found behavior. We can therefore rule out this latter possibility.

In Fig. S6, we compare $d_{1,2}(\mathcal{N})$ with different scalings of the form $\sqrt{\mathcal{N}}/\ln^{n-1}\mathcal{N}$, for $n = 1, 2, 3$. The tendency of the data for large $\mathcal{N}$ seems to be best described by the case $n = 2$, which implies that most likely the dominant finite-size correction to $\langle \tilde{D}_{1,2} \rangle$ is exactly described by GOE while the next term is of the form $1/\ln^2\mathcal{N}$.